Partial muon capture rates in $A = 3$ and $A = 6$ nuclei with chiral effective field theory

G. B. King[a], S. Pastore[a,b], M. Piarulli[a,b], R. Schiavilla[c,d]

[a]*Department of Physics, Washington University in Saint Louis, Saint Louis, MO 63130, USA*
[b]*McDonnell Center for the Space Sciences at Washington University in St. Louis, MO 63130, USA*
[c]*Department of Physics, Old Dominion University, Norfolk, VA 23529, USA*
[d]*Theory Center, Jefferson Lab, Newport News, VA 23606, USA*
(Dated: April 19, 2022)

Searches for neutrinoless-double beta decay rates are crucial in addressing questions within fundamental symmetries and neutrino physics. The rates of these decays depend not only on unknown parameters associated with neutrinos, but also on nuclear properties. In order to reliably extract information about the neutrino, one needs an accurate treatment of the complex many-body dynamics of the nucleus. Neutrinoless-double beta decays take place at momentum transfers on the order of 100 MeV/c and require both nuclear electroweak vector and axial current matrix elements. Muon capture, a process in the same momentum transfer regime, has readily available experimental data to validate these currents. In this work, we present results of *ab initio* calculations of partial muon capture rates for ^{3}He and ^{6}Li nuclei using variational and Green's Function Monte Carlo computational methods. We estimate the impact of the three-nucleon interactions, the cutoffs used to regularize two-nucleon ($2N$) interactions, and the energy range of $2N$ scattering data used to fit these interactions.

Introduction, conclusions and outlook. Nuclei play a crucial role in high-precision tests of the Standard Model and searches for physics beyond the Standard Model. These investigations, including neutrinoless double beta decay ($0\nu\beta\beta$) searches [1] and high-precision beta decay experiments [2–4], require a thorough understanding of standard nuclear effects in order to separate them from new physics signals. In particular, $0\nu\beta\beta$ decay experiments aim to establish the origin and nature of neutrino masses and test leptogenesis scenarios leading to the observed matter-antimatter asymmetry in the universe [1]. Rates of these decays depend not only on unknown neutrino parameters but also on nuclear matrix elements. The latter can be provided only from theoretical calculations. Thus, a prerequisite to this experimental program is an accurate treatment of the complex many-body dynamics of the nucleus and its interactions with neutrinos. If one assumes that $0\nu\beta\beta$ decay results come from the exchange of a light Majorana neutrino between two nucleons, then the momentum carried by the neutrino is on the order of 100 MeV/c [1, 5]. Muon captures on nuclei—processes where a muon captures on a proton in the nucleus releasing a neutron and a neutrino—involve momentum transfers on the order of the muon mass. The scope of this work is to validate our nuclear model in this kinematic regime by calculating muon capture rates in $A = 3$ and $A = 6$ nuclei for comparison with available experimental data.

Muon capture reactions have been treated extensively from both the theoretical and experimental points of view [6–9] and rates have been obtained in light systems with several methods [10–21]. Here, we present calculations of partial muon capture rates using quantum Monte Carlo methods (QMC) [22]—both variational (VMC) and Green's function Monte Carlo (GFMC) methods—

to solve the nuclear many-body problem. QMC methods allow one to fully retain the complexity of many-body physics and have been successfully applied to study many nuclear electroweak properties over a wide range of energy and momentum transfer, including total muon capture rates in ^{3}H and ^{4}He [23], low-energy electroweak transitions [24–28], nuclear responses induced by electrons and neutrinos [29–31], neutrinoless double beta decay matrix elements [5, 32–34], and matrix elements for dark matter scattering [35].

The Norfolk two-nucleon ($2N$) and three-nucleon ($3N$) (NV2+3) local chiral interactions [36–39] have been used in combination with QMC methods to study static properties of light nuclei [37, 40–43], and in auxiliary-field diffusion Monte Carlo [44], Brueckner-Bethe-Goldstone [45, 46] and Fermi hypernetted chain/single-operator chain [47, 48] approaches to investigate the equation of state of neutron matter [49, 50]. Reference [51], a study which included the current authors, reports on Gamow-Teller (GT) matrix elements calculated for $A \leq 10$ nuclei using the NV2+3 models and their consistent axial-vector currents at tree-level from Refs. [38, 39, 52]. The study validated the many-body interactions and currents in the limit of vanishing momentum transfer. In the present work, we use the same nuclear Hamiltonians and axial currents, along with chiral vector currents retaining loop corrections developed in Refs. [24, 25, 53, 54], to test the model at moderate momentum transfers on the order of 100 MeV/c and to assess the sensitivity of partial muon capture rates to the dynamical input.

In the $A = 3$ system, we obtain an average rate for all Norfolk models of $\Gamma(A = 3; \text{VMC}) = 1512 \pm 32$ s^{-1} at the VMC level that agrees with the experimental result of 1496.0 ± 4.0 s^{-1} [55] within error bar. In the $A = 6$ system,

the VMC partial capture rate of $\Gamma(A=6; \text{VMC}) = 1243 \pm 59 \ s^{-1}$ is significantly slower than the available experimental data point of $1600^{+330}_{-129} \ s^{-1}$ [56], but falls into the range of previous theoretical estimates [57–63]. We analyzed uncertainties due to (i) the choice of cutoffs used to regularize the NV2 interactions, (ii) the energy range of $2N$ scattering data used to fit the model low-energy constants (LECs), (iii) two different versions of NV3 interactions, $i.e.$, the non-starred model fit to the nd scattering length and the trinucleon binding energies, and the starred model fit to the triton GT matrix element and the trinucleon binding energies, and (iv) a 10% variation in the nucleonic axial radius. In the $A=3$ system, the largest source of uncertainty comes from the choice of $3N$ interaction model, while for $A=6$ we find that the uncertainty due to the $3N$ interaction is slightly less than, but on the order of, the cutoff and energy range uncertainties. On average, there is a change in the rate by $\pm 0.6\%$ when the axial radius is varied in the interval $r_A = [0.5859, 0.7161]$ fm.

We improved upon our VMC estimate by performing GFMC propagations using models NV2+3-Ia and NV2+3-Ia*, or Ia and Ia* for short, in both the $A=3$ and $A=6$ systems. These models share the same $2N$ interaction, but differ in how the $3N$ interaction is fit with $(c_D, c_E) = (3.666, -1.638)$ for Ia [40] and $(c_D, c_E) = (-0.635, -0.090)$ for Ia* [39]. Model Ia, constrained by strong interaction data only, achieves 1.5% agreement with the experimental datum for $A=3$ with a calculated rate of $1519 \pm 3 \ s^{-1}$. Its counterpart, model Ia*, constrained to both strong and electroweak data, underpredicts the experimental rate by a few percent. For $A=6$, we find that the model Ia* propagation significantly decreases the rate due to the monotonic growth of the ^{6}He ground state rms radius at early imaginary times. By contrast, model Ia has a stable radius throughout the GFMC propagation and the rate decreases by less than 1%; nevertheless, it still underpredicts the experimental datum.

Given the large error bars on the ^{6}Li datum and the wide range of values from past theoretical calculations, we advocate for renewed experimental and theoretical attention to this partial capture rate. While in this letter we focus on ^{3}He and ^{6}Li to demonstrate the impact of this sort of study, there are other muon capture rates with available experimental data which the combination of QMC methods and NV2+3 chiral Hamiltonians could be made to address with future development; examples are ^{10}B, ^{11}B, ^{12}C, ^{16}O, and ^{40}Ca [7]. Calculations of these rates, particularly for the heavier nuclei, would be valuable in further validating the present *ab initio* approach in the kinematic regime relevant to neutrinoless double beta decay.

Partial muon capture rate. The muon capture processes $^3\text{He}(\mu^-, \nu_\mu)^3\text{H}$ and $^6\text{Li}(\mu^-, \nu_\mu)^6\text{He}$ are induced by the weak-interaction Hamiltonian H_W [64, 65]

$$\langle \mathbf{k}_\nu, h_\nu | H_W | \mathbf{k}_\mu, s_\mu \rangle = \frac{G_V}{\sqrt{2}} \int d^3 x e^{-i\mathbf{k}_\nu \cdot \mathbf{x}} \tilde{l}_\sigma(\mathbf{x}) j^\sigma(\mathbf{x}) , \tag{1}$$

where $G_V = G_F \cos\theta_C = 1.1363 \times 10^{-5} \ \text{GeV}^{-2}$ is the Fermi coupling constant extracted from analyses of superallowed β-decays [66], j^σ and $\tilde{l}_\sigma$ are the hadronic and leptonic four-current density operators [10], s_μ is the muon spin, h_ν is the neutrino helicity, and $\mathbf{k}_\mu$ and $\mathbf{k}_\nu$ are the muon and neutrino momenta, respectively. The value of G_V adopted here is from a more recent analysis and is $\sim 1.1\%$ smaller than that used in previous calculations based on the hyperspherical harmonics method with chiral currents from Ref. [12].

For a transition from an initial nuclear state $|i, J_i M_i\rangle$—where $J_{i/f}$ and $M_{i/f}$ denote the nuclear spin and its projection—to a final nuclear state $|f, J_f M_f, -\mathbf{k}_\nu\rangle$ recoiling with momentum $-\mathbf{k}_\nu$, the general expression for the capture rate (Γ), summed over the final states and averaged over the initial states, is given (in the limit of vanishing $\mathbf{k}_\mu$) by [10, 64, 65]

$$d\Gamma = \frac{1}{2(2J_i + 1)} \sum_{s_\mu, M_i} \sum_{h_\nu, M_f} 2\pi \delta(\omega) \tag{2}$$

$$\times |\langle \mathbf{k}_\nu, h_\nu; f, J_f M_f, -\mathbf{k}_\nu | H_W | s_\mu; i, J_i M_i \rangle|^2 \frac{d^3 k_\nu}{(2\pi)^3} ,$$

where the argument of the δ-function is

$$\omega = E_\nu + \sqrt{E_\nu^2 + (m_f + E_f)^2} - (m_\mu + m_i + E_i) , \tag{3}$$

and E_i and E_f are the initial and final state energies of the nucleus [67–69]—we have neglected internal electronic energies, since they are of the order of tens of eV's for the light atoms under consideration. We also used the following definitions

$$\begin{aligned} m_i &= Z m_p + N m_n + (Z - 1) m_e , \\ m_f &= (Z - 1)(m_p + m_e) + (N + 1) m_n , \end{aligned} \tag{4}$$

for an initial nucleus with charge number Z and neutron number N, and we denoted with m_p, m_n, and m_e the proton, neutron, and electron masses, respectively.

The final integrated rate can be conveniently written in terms of matrix elements of the nuclear electroweak current components [11],

$$\Gamma = \frac{G_V^2}{2\pi} \frac{|\psi_{1s}^{\mathrm{av}}|^2}{(2J_i+1)} \frac{E_\nu^{*2}}{\mathrm{recoil}} \sum_{M_f, M_i} \left[|\langle J_f, M_f | \rho(E_\nu^* \hat{\mathbf{z}}) | J_i, M_i \rangle|^2 + |\langle J_f, M_f | j_z(E_\nu^* \hat{\mathbf{z}}) | J_i, M_i \rangle|^2 \right.$$

$$+ 2\mathrm{Re}\left[\langle J_f, M_f | \rho(E_\nu^* \hat{\mathbf{z}}) | J_i, M_i \rangle \langle J_f, M_f | j_z(E_\nu^* \hat{\mathbf{z}}) | J_i, M_i \rangle^* \right] + |\langle J_f, M_f | j_x(E_\nu^* \hat{\mathbf{z}}) | J_i, M_i \rangle|^2$$

$$+ |\langle J_f, M_f | j_y(E_\nu^* \hat{\mathbf{z}}) | J_i, M_i \rangle|^2 - 2\,\mathrm{Im}\left[\langle J_f, M_f | j_x(E_\nu^* \hat{\mathbf{z}}) | J_i, M_i \rangle \langle J_f, M_f | j_y(E_\nu^* \hat{\mathbf{z}}) | J_i, M_i \rangle^* \right] \right] , \tag{5}$$

where we have chosen $\hat{\mathbf{k}}_\nu = -\hat{\mathbf{z}}$, and have introduced the outgoing neutrino energy [11]

$$E_\nu^* = \frac{(m_i + E_i + m_\mu)^2 - (m_f + E_f)^2}{2(m_i + E_i + m_\mu)} , \tag{6}$$

and recoil factor

$$\frac{1}{\mathrm{recoil}} = \left(1 - \frac{E_\nu^*}{m_i + E_i + m_\mu} \right) . \tag{7}$$

The factor $|\psi_{1s}^{\mathrm{av}}|^2$ is written as $\mathcal{R}\,|\psi_{1s}(0)|^2$, where $\psi_{1s}(0)$ is the 1s wave function, evaluated at the origin, of a hydrogen-like atom, and $\mathcal{R}$ approximately accounts for the finite size of the nuclear charge distribution [11], here calculated with the NV2+3 Hamiltonians.

Nuclear Hamiltonians and electroweak currents. To calculate the nuclear matrix elements required by Eq. (5) we employ VMC [70] and GFMC [71] methods. For a comprehensive review of these methods, see Refs. [22, 41] and references therein. Details about the calculation of matrix elements using GFMC wave functions are found in Eqs. (19)–(24) of Ref. [72].

The many-body Hamiltonian is composed of a (one-body) kinetic energy term, and the Norfolk $2N$ and $3N$ local interactions that include N3LO and N2LO terms in the chiral expansion, respectively. Details about the derivation of the interaction in chiral effective field theory can be found in Ref. [36–39]. Here, we briefly summarize the differences between the model classes employed in this work. Models in class I (II) fit the $2N$ interaction to about 2700 (3700) data points up to lab energy of 125 (200) MeV in the nucleon-nucleon scattering database with a χ^2/datum of about $\lesssim 1.1$ ($\lesssim 1.4$). Within each class, models a and b differ in the set of cutoffs adopted to regularize the short- and long-range components of the interaction, either $(R_S, R_L) = (0.8, 1.2)$ fm for model a or $(R_S, R_L) = (0.7, 1.0)$ fm for model b [36, 37]. The different fitting procedures result in different values for the 26 unknown LECs governing the strength of short-range terms in the interactions. Accompanying these $2N$ interactions is the leading chiral $3N$ interaction which introduces two unknown LECs c_D and c_E (in standard notation) constrained to reproduce the trinucleon binding energies and, concurrently, either the GT matrix element contributing to tritium β-decay [39] in the starred model or the *nd*-doublet scattering length in the non-starred one [40].

Lastly, the vector- and axial-current operators entering the calculation were derived with time-ordered perturbation theory by the JLab-Pisa group using the same χEFT formulation as the NV2+3 interactions. Details about the electroweak currents used in this work can be found in Refs. [24, 25, 38, 39, 52–54].

Results. The results of the VMC calculation of the partial muon capture rate in $A = 3$ and $A = 6$ using the NV2+3 nuclear Hamiltonian are presented in Table I. Capture rates were determined using nuclear axial and vector current operators consistent with the NV2+3 model. The nuclear axial currents [38] contain only tree-level diagrams while the vector current operators account for loop corrections derived in Ref. [24, 25, 53, 54].

Calculations of the rate with the leading order one-body only $[\Gamma(1b)]$ and one- plus two-body electroweak currents $[\Gamma(2b)]$ were performed for ground-state to ground-state transitions. The partial capture rate on ^{3}He has been precisely measured [55] and the one-body contribution alone cannot reproduce this measurement. With the two-body electroweak currents included, the VMC rates increase by about 9% to 16%. At this level, the agreement with the datum ranges from about 0.1% to 4.6%. How the $3N$ interaction was fit has the most significant impact on the rate, leading to differences on average of $54\,\mathrm{s}^{-1}$ whenever the $3N$ interaction is changed. Note that the LEC c_D entering the $3N$ interaction governs the strength of the axial contact current at next-to-next-to-next-to-leading order in the chiral expansion [51]. Therefore, variations in the $3N$ interaction lead to variations in the current, as also observed in the study of Ref. [51] on beta decay matrix elements. The cutoff and energy range of the fit lead to changes of $16\,\mathrm{s}^{-1}$ and $22\,\mathrm{s}^{-1}$ on average, respectively, which is consistent with the findings of Refs. [12, 15].

In the ^{6}Li capture, the inclusion of two-body electroweak currents also increases the rate with a greater enhancement in the non-starred models relative to their starred counterparts. Even with this increase, ranging approximately from 3% to 7%, the rates predicted at the VMC level for the NV2+3 models are about 11–21% slower than the available experimental datum [56]. Here, the difference due to the $3N$ interaction is no longer the dominant contribution to the uncertainty. We find that, on average, the cutoff and energy range of the fit both change the rate by $72\,\mathrm{s}^{-1}$, while the $3N$ interaction changes the rate by $60\,\mathrm{s}^{-1}$.

We compute a VMC average for both rates under study

and use the average changes due to the chiral $2N$ interaction cutoffs, the energy range used to fit the interaction, and the $3N$ interaction to assign a total error bar. An additional source of uncertainty was considered by varying the nucleonic axial radius parameter by $\pm 10\%$. We found that, on average, the difference in the rate was $\pm 0.6\%$ due to this variation. We combine the four uncertainties in quadrature to determine the overall uncertainty on the VMC averages, obtaining $\Gamma(A=3; \mathrm{VMC}) = 1512 \pm 32$ s^{-1} and $\Gamma(A=6; \mathrm{VMC}) = 1243 \pm 59$ s^{-1}.

In addition to the VMC calculation, a GFMC propagation was performed for models Ia and Ia*, and corresponding results are reported in Table II. These two models provided the fastest and slowest VMC partial capture rates for $A=3$ and should give an upper and lower limit on GFMC rates. The GFMC method removes spurious contamination from the VMC wave functions by propagating them in imaginary time τ and should thus provide more reliable results for these two nuclear Hamiltonians. Figure 1 displays our average VMC results, as well as both VMC and GFMC results for models Ia and Ia*, compared with experimental data and past theoretical calculations. The GFMC error is taken to be half the difference between the two available calculations.

At the VMC level, model Ia overpredicted the $A=3$ muon capture rate by 4.6%. After propagation, the rate is decreased and reaches a 1.5% agreement with the datum. By contrast, model Ia*, which had 1.4% agreement with the experimental datum at the VMC level, now underpredicts the rate by 4.2%.

In Fig. 1 panel (a), one sees that the results of past chiral calculations in Refs. [12] and [15] fall within the bounds for the NV2+3 GFMC rate provided by models Ia and Ia*. Even when using the more recent value of G_V, the rate of [12] falls within our GFMC band. While there is this agreement, because these past calculations use a different set of chiral currents and underlying nuclear interactions than the present work, it is difficult to directly compare them to our GFMC results. In the future, benchmark calculations with other *ab initio* methods based on the same dynamical inputs would be useful to further validate the present microscopic approach.

While the $A=3$ GFMC rates exhibit few-percent decreases from the VMC ones, the $A=6$ rates display a dramatically different behavior for models Ia and Ia*. The matrix elements for the model Ia calculation were fairly stable when propagated from VMC to GFMC, resulting in a modest sub-percent change of the overall rate. However, for model Ia*, the dominant matrix elements changed at the few percent level, but since the rate is proportional to the square of the matrix element, this leads to a change of roughly 20% in the rate.

To further understand this behavior, one can look at the system size as a function of τ during the GFMC propagation of the $A=6$ nuclei. The system size for ^{6}Li$(1^+; 0)$ grows at the same rate in τ for both models; however, the ^{6}He$(0^+; 1)$ ground state size is stable for model Ia while increasing monotonically in τ before beginning to
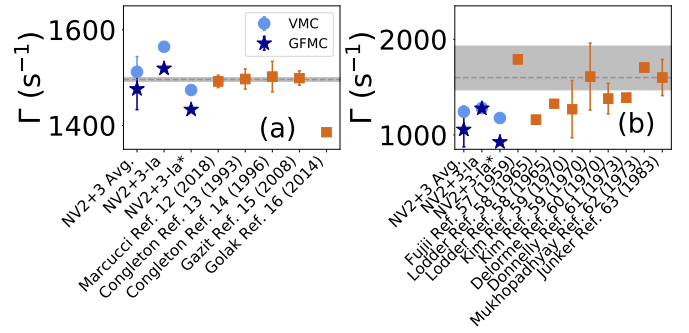

FIG. 1. The partial muon capture rate in (a) ^{3}He and (b) ^{6}Li from the the NV2+3-Ia and NV2+3-Ia* models in VMC (light blue circle) and GFMC (dark blue star) calculations compared with other work (orange squares) [12–15, 57–63]. The experimental values (dashed gray line) and their error (shaded region) [55, 56] are included for comparison with the theory predictions.

converge for model Ia* (see Supplemental Material [73]). Because of the $e^{-i\mathbf{q}\cdot\mathbf{r}_i}$ dependence in the dominant one-body terms of the current operator, the matrix elements at a finite value of q experience a more significant drop for model Ia* due to the diffuseness of ^{6}He$(0^+; 1)$ with that interaction. Performing the same analysis for the $A=3$ system, we find that the system size is consistent between both models as a function of τ, explaining the similarity in their decreasing trend for this partial muon capture rate.

The difference with experiment in $A=6$ is significant for both models Ia and Ia*, especially when compared with the few percent agreement obtained in GFMC calculations of the GT matrix element for the ^{6}He $\rightarrow$ ^{6}Li beta decay [51]. As detailed in Ref. [63], calculations of this rate [57–63] have ranged from 1160 s^{-1} to 1790 s^{-1}. The calculation of Ref. [63] matched the experimental datum by modelling ^{6}Li as a ^{3}He + t cluster and using the Fujii-Primakoff [57] effective Hamiltonian for muon capture. Sub-percent agreement was also obtained by Ref. [59], which treated the ^{6}Li and ^{6}He nuclei as elementary particles with magnetic and axial form factors extracted from experiment. The two calculations presented by the authors of that work adopted different formulations of the partially conserved axial current (PCAC) relation to obtain the pseudoscalar form factor, with the faster rate using the Gell-Mann-Lévy version [74] and the slower rate using the Nambu one [75]. The Nambu definition is consistent with the induced pseudoscalar term in the weak axial current from χEFT.

It is difficult to compare our result with those of other theoretical treatments of the ^{6}Li partial capture rate, particularly since most of these treatments are decades old. For example, in the work of Ref. [61] the weak-interaction Hamiltonian is that of Eq. (1); however, the ^{6}Li and ^{6}He bound states are described by shell-model wave functions with valence configurations restricted to

Capture	Model	$\mathcal{R}$	Γ(1b) (s^{-1})	Γ(2b) (s^{-1})	Expt. (s^{-1})
^{3}He($\frac{1}{2}^+$;$\frac{1}{2}$) $\to$ ^{3}H($\frac{1}{2}^+$;$\frac{1}{2}$)	Ia (Ib)	0.995 (0.995)	1350.3 $\pm$ 0.8 (1363.4 $\pm$ 0.2)	1564.4 $\pm$ 0.9 (1545.7 $\pm$ 0.3)	1496.0 $\pm$ 4.0 [55]
	Ia* (Ib*)	0.995 (0.995)	1357.4 $\pm$ 0.2 (1358.5 $\pm$ 0.2)	1473.9 $\pm$ 0.3 (1483.6 $\pm$ 0.3)	
	IIa (IIb)	0.995 (0.995)	1369.7 $\pm$ 0.2 (1372.8 $\pm$ 0.2)	1533.8 $\pm$ 0.3 (1512.4 $\pm$ 0.3)	
	IIa* (IIb*)	0.995 (0.995)	1364.5 $\pm$ 0.2 (1372.5 $\pm$ 0.2)	1484.4 $\pm$ 0.3 (1497.0 $\pm$ 0.3)	
^{6}Li(1^+;0) $\to$ ^{6}He(0^+;1)	Ia (Ib)	0.990 (0.990)	1196 $\pm$ 2 (1243 $\pm$ 2)	1282 $\pm$ 2 (1331 $\pm$ 2)	1600$^{+330}_{-129}$ [56]
	Ia* (Ib*)	0.990 (0.990)	1154 $\pm$ 3 (1188 $\pm$ 2)	1177 $\pm$ 3 (1233 $\pm$ 2)	
	IIa (IIb)	0.990 (0.990)	1227 $\pm$ 2 (1142 $\pm$ 2)	1294 $\pm$ 2 (1185 $\pm$ 2)	
	IIa* (IIb*)	0.990 (0.990)	1215 $\pm$ 2 (1151 $\pm$ 2)	1257 $\pm$ 2 (1185 $\pm$ 2)	

TABLE I. VMC calculations of partial muon capture rates in ^{3}He and ^{6}Li obtained with chiral one-body only [Γ(1b)], and one- and two-body [Γ(2b)] axial and vector currents corresponding to the eight NV2+3 models. The third column gives the factor $\mathcal{R}$ used to account for the finite nuclear charge distribution. The experimental result is given in the last column. All uncertainties on the theoretical predictions are Monte Carlo errors.

Capture	Model	Γ(VMC) (s^{-1})	Γ(GFMC) (s^{-1})	Expt.
^{3}He($\frac{1}{2}^+$;$\frac{1}{2}$) $\to$ ^{3}H($\frac{1}{2}^+$;$\frac{1}{2}$)	Ia	1564.4 $\pm$ 0.9	1519 $\pm$ 3	1496.0 $\pm$ 4.0 [55]
	Ia*	1473.9 $\pm$ 0.3	1433 $\pm$ 2	
^{6}Li(1^+;0) $\to$ ^{6}He(0^+;1)	Ia	1282 $\pm$ 2	1277 $\pm$ 10	1600 $^{+330}_{-129}$ [56]
	Ia*	1177 $\pm$ 2	926 $\pm$ 8	

TABLE II. VMC and GFMC calculations of partial muon capture rates in ^{3}He and ^{6}Li obtained with chiral one- and two-body axial and vector currents with the NV2+3 models. The experimental result is given in the last column. All uncertainties on the theoretical predictions are Monte Carlo errors.

the 1p-shell; moreover, the nuclear electroweak current neglects meson-exchange contributions [61]. We find that our result at leading order (obtained with one-body currents) is quenched relative to the shell model one, as we would have expected (see Ref. [51]). More modern calculations with other *ab initio* methods and a novel measurement of the rate would be valuable in establishing the validity of our nuclear inputs and many-body approach.

[1] J. Engel and J. Menéndez, Reports on Progress in Physics **80**, 046301 (2017).

[2] M. Gonzalez-Alonso, O. Naviliat-Cuncic, and N. Severijns, Prog. Part. Nucl. Phys. **104**, 165 (2019), arXiv:1803.08732 [hep-ph].

[3] V. Cirgiliano, A. Garcia, D. Gazit, O. Naviliat-Cuncic, G. Savard, and A. Young, Precision beta decay as a probe of new physics (2019), arXiv:1907.02164 [nucl-ex].

[4] A. Glick-Magid, C. Forssén, D. Gazda, D. Gazit, P. Gysbers, and P. Navrátil, (2021), arXiv:2107.10212 [nucl-th].

[5] S. Pastore, J. Carlson, V. Cirigliano, W. Dekens, E. Mereghetti, and R. B. Wiringa, Physical Review C

97, 014606 (2018), arXiv:1710.05026.

[6] N. C. Mukhopadhyay, Physics Reports **30**, 1 (1977).

[7] D. Measday, Physics Reports **354**, 243 (2001).

[8] P. Kammel and K. Kubodera, Annual Review of Nuclear and Particle Science **60**, 327 (2010), https://doi.org/10.1146/annurev-nucl-100809-131946.

[9] T. Gorringe and D. Hertzog, Progress in Particle and Nuclear Physics **84**, 73 (2015), arXiv:1506.01465.

[10] L. E. Marcucci, R. Schiavilla, S. Rosati, A. Kievsky, and M. Viviani, Phys. Rev. C **66**, 054003 (2002), arXiv:nucl-th/0112008.

[11] L. E. Marcucci, M. Piarulli, M. Viviani, L. Girlanda, A. Kievsky, S. Rosati, and R. Schiavilla, Phys. Rev. C **83**, 014002 (2011).

[12] L. E. Marcucci, A. Kievsky, S. Rosati, R. Schiavilla, and M. Viviani, Phys. Rev. Lett. **108**, 052502 (2012), [Erratum: Phys. Rev. Lett.121,no.4,049901(2018)], arXiv:1109.5563 [nucl-th].

[13] J. Congleton and H. Fearing, Nuclear Physics A **552**, 534 (1993).

[14] J. G. Congleton and E. Truhlík, Phys. Rev. C **53**, 956 (1996).

[15] D. Gazit, Phys. Lett. B **666**, 472 (2008), arXiv:0803.0036 [nucl-th].

[16] J. Golak, R. Skibiński, H. Witała, K. Topolnicki, A. E. Elmeshneb, H. Kamada, A. Nogga, and L. E. Marcucci, Phys. Rev. C **90**, 024001 (2014).

[17] J. Adam, M. Tater, E. Truhlík, E. Epelbaum, R. Machleidt, and P. Ricci, Physics Letters, Section B: Nuclear, Elementary Particle and High-Energy Physics **709**, 93 (2012), arXiv:1110.3183.

[18] E. Kolbe, K. Langanke, and P. Vogel, Phys. Rev. C **50**, 2576 (1994).

[19] T. Marketin, N. Paar, T. Nikšić, and D. Vretenar, Phys. Rev. C **79**, 054323 (2009).

[20] A. R. Samana, F. Krmpotić, N. Paar, and C. A. Bertulani, Phys. Rev. C **83**, 024303 (2011).

[21] P. G. Giannaka and T. S. Kosmas, Phys. Rev. C **92**, 014606 (2015).

[22] J. Carlson, S. Gandolfi, F. Pederiva, S. C. Pieper, R. Schiavilla, K. E. Schmidt, and R. B. Wiringa, Rev. Mod. Phys. **87**, 1067 (2015), arXiv:1412.3081 [nucl-th].

[23] A. Lovato, N. Rocco, and R. Schiavilla, Phys. Rev. C **100**, 035502 (2019).

[24] S. Pastore, L. Girlanda, R. Schiavilla, M. Viviani, and R. B. Wiringa, Phys. Rev. C **80**, 034004 (2009).

[25] S. Pastore, L. Girlanda, R. Schiavilla, and M. Viviani, Phys. Rev. C **84**, 024001 (2011).

[26] S. Pastore, S. C. Pieper, R. Schiavilla, and R. B. Wiringa, Phys. Rev. C **87**, 035503 (2013).

[27] S. Pastore, R. B. Wiringa, S. C. Pieper, and R. Schiavilla, Physical Review C - Nuclear Physics **90**, 024321 (2014).

[28] S. Pastore, A. Baroni, J. Carlson, S. Gandolfi, S. C. Pieper, R. Schiavilla, and R. B. Wiringa, Phys. Rev. C **97**, 022501(R) (2018).

[29] A. Lovato, S. Gandolfi, J. Carlson, E. Lusk, S. C. Pieper, and R. Schiavilla, Phys. Rev. C **97**, 022502(R) (2018).

[30] A. Lovato, J. Carlson, S. Gandolfi, N. Rocco, and R. Schiavilla, (2020).

[31] S. Pastore, J. Carlson, S. Gandolfi, R. Schiavilla, and R. B. Wiringa, Phys. Rev. C **101**, 044612 (2020), arXiv:1909.06400 [nucl-th].

[32] V. Cirigliano, W. Dekens, J. de Vries, M. L. Graesser, E. Mereghetti, S. Pastore, and U. van Kolck, Phys. Rev.

Lett. **120**, 202001 (2018).

[33] V. Cirigliano, W. Dekens, J. de Vries, M. L. Graesser, E. Mereghetti, S. Pastore, M. Piarulli, U. van Kolck, and R. B. Wiringa, Physical Review C **100**, 055504 (2019).

[34] X. B. Wang, A. C. Hayes, J. Carlson, G. X. Dong, E. Mereghetti, S. Pastore, and R. B. Wiringa, Physics Letters, Section B: Nuclear, Elementary Particle and High-Energy Physics **798**, 134974 (2019), arXiv:1906.06662.

[35] L. Andreoli, V. Cirigliano, S. Gandolfi, and F. Pederiva, Phys. Rev. C **99**, 025501 (2019), arXiv:1811.01843 [nucl-th].

[36] M. Piarulli, L. Girlanda, R. Schiavilla, R. N. Pérez, J. E. Amaro, and E. R. Arriola, Phys. Rev. **C91**, 024003 (2015), arXiv:1412.6446 [nucl-th].

[37] M. Piarulli, L. Girlanda, R. Schiavilla, A. Kievsky, A. Lovato, L. E. Marcucci, S. C. Pieper, M. Viviani, and R. B. Wiringa, Phys. Rev. **C94**, 054007 (2016), arXiv:1606.06335 [nucl-th].

[38] A. Baroni, L. Girlanda, A. Kievsky, L. E. Marcucci, R. Schiavilla, and M. Viviani, Phys. Rev. **C94**, 024003 (2016), [Erratum: Phys. Rev.C95,no.5,059902(2017)], arXiv:1605.01620 [nucl-th].

[39] A. Baroni, R. Schiavilla, L. E. Marcucci, L. Girlanda, A. Kievsky, A. Lovato, S. Pastore, M. Piarulli, S. C. Pieper, M. Viviani, and R. B. Wiringa, Phys. Rev. C **98**, 044003 (2018).

[40] M. Piarulli, A. Baroni, L. Girlanda, A. Kievsky, A. Lovato, E. Lusk, L. E. Marcucci, S. C. Pieper, R. Schiavilla, M. Viviani, and R. B. Wiringa, Phys. Rev. Lett. **120**, 052503 (2018).

[41] J. Lynn, I. Tews, S. Gandolfi, and A. Lovato, Annual Review of Nuclear and Particle Science **69**, 279 (2019), https://doi.org/10.1146/annurev-nucl-101918-023600.

[42] M. Piarulli and I. Tews, Frontiers in Physics **7**, 245 (2020).

[43] S. Gandolfi, D. Lonardoni, A. Lovato, and M. Piarulli, Frontiers in Physics **8**, 117 (2020).

[44] K. E. Schmidt and S. Fantoni, Phys. Lett. **B446**, 99 (1999).

[45] B. D. Day, Rev. Mod. Phys. **39**, 719 (1967).

[46] M. Baldo and G. F. Burgio, Rep. Progr. Phys. **75**, 026301 (2012).

[47] S. Fantoni and S. Rosati, Nuovo Cimento A **25**, 593 (1975).

[48] V. R. Pandharipande and R. B. Wiringa, Rev. Mod. Phys. **51**, 821 (1979).

[49] M. Piarulli, I. Bombaci, D. Logoteta, A. Lovato, and R. B. Wiringa, (2019), arXiv:1908.04426 [nucl-th].

[50] I. Bombaci and D. Logoteta, Astron. Astrophys. **609**, A128 (2018), arXiv:1805.11846 [astro-ph.HE].

[51] G. B. King, L. Andreoli, S. Pastore, M. Piarulli, R. Schiavilla, R. B. Wiringa, J. Carlson, and S. Gandolfi, Phys. Rev. C **102**, 025501 (2020), arXiv:2004.05263 [nucl-th].

[52] A. Baroni, L. Girlanda, S. Pastore, R. Schiavilla, and M. Viviani, Phys. Rev. **C93**, 015501 (2016), [Erratum: Phys. Rev.C95,no.5,059901(2017)], arXiv:1509.07039 [nucl-th].

[53] S. Pastore, R. Schiavilla, and J. L. Goity, Phys. Rev. C **78**, 064002 (2008).

[54] R. Schiavilla, A. Baroni, S. Pastore, M. Piarulli, L. Girlanda, A. Kievsky, A. Lovato, L. E. Marcucci, S. C. Pieper, M. Viviani, and R. B. Wiringa, Phys. Rev. C **99**, 034005 (2019).

[55] P. Ackerbauer, D. Balin, V. Baturin, G. Beer, W. Breunlich, T. Case, K. Crowe, H. Daniel, J. Deutsch, J. Govaerts, Y. Grigoriev, F. Hartmann, P. Kammel, R. King, B. Lauss, E. Maev, V. Markushin, J. Marton, M. Mühlbauer, C. Petitjean, T. Petitjean, G. Petrov, R. Prieels, W. Prymas, W. Schott, G. Semenchuk, Y. Smirenin, A. Vorobyov, N. Voropaev, and P. Wojciechowski, Physics Letters B **417**, 224 (1998).

[56] J. Deutsch, L. Grenacs, P. Igo-Kemenes, P. Lipnik, and P. Macq, Physics Letters B **26**, 315 (1968).

[57] A. Fujii and H. Primakoff, Il Nuovo Cimento (1955-1965) **12**, 327 (1959).

[58] A. Lodder and C. Jonker, Physics Letters **15**, 245 (1965).

[59] C. Kim and S. Mintz, Physics Letters B **31**, 503 (1970).

[60] J. Delorme, Nuclear Physics B **19**, 573 (1970).

[61] T. Donnelly and J. Walecka, Physics Letters B **44**, 330 (1973).

[62] N. Mukhopadhyay, Physics Letters B **45**, 309 (1973).

[63] K. Junker, Nuclear Physics A **407**, 460 (1983).

[64] J. D. Walecka, in *Muon Physics: Weak Interactions*, edited by V. W. Hughes and C. S. Wu (Academic, New York, 1975).

[65] J. D. Walecka, *Theoretical Nuclear and Subnuclear Physics* (Oxford University Press, New York, 1995).

[66] J. C. Hardy and I. S. Towner, Phys. Rev. C **91**, 025501 (2015).

[67] J. Purcell and C. Sheu, Nuclear Data Sheets **130**, 1 (2015).

[68] D. Tilley, C. Cheves, J. Godwin, G. Hale, H. Hofmann, J. Kelley, C. Sheu, and H. Weller, Nuclear Physics A **708**, 3 (2002).

[69] J. Kelley, J. Purcell, and C. Sheu, Nuclear Physics A **968**, 71 (2017).

[70] R. B. Wiringa, Phys. Rev. **C43**, 1585 (1991).

[71] J. Carlson and R. Schiavilla, Rev. Mod. Phys. **70**, 743 (1998).

[72] M. Pervin, S. C. Pieper, and R. B. Wiringa, Phys. Rev. C **76**, 064319 (2007).

[73] See Supplemental Material at [URL] for plots of the point proton rms radii of the $A = 3$ and $A = 6$ systems as functions of τ during GFMC propagation.

[74] M. Gell-Mann and M. Levy, Nuovo Cim. **16**, 705 (1960).

[75] Y. Nambu, Phys. Rev. Lett. **4**, 380 (1960).

Supplemental Material

This supplemental material is provided to show how the system sizes of the $A=3$ and $A=6$ nuclei evolve during GFMC propagation in imaginary time τ. As noted in the text, the system size of ^{6}He(0^+; 1) has a different imaginary time behavior for models Ia and Ia*. While it remains stable for model Ia, the system size grows monotonically in τ for model Ia*. Because of this difference and the $e^{i\mathbf{q}\cdot\mathbf{r}_i}$ dependence of the dominant one-body current operators, the transition matrix elements for this system experience a larger decrease in model Ia* compared to model Ia. This, in turn, leads to the larger drop in the rate going from VMC to GFMC for model Ia* relative to its counterpart. For ^{6}Li(1^+; 0) and the $A=3$ ground states, the system size in τ is consistent between models Ia and Ia*. Figures 2 and 3 display the rms point proton radii of the $A=3$ and $A=6$ systems, respectively.
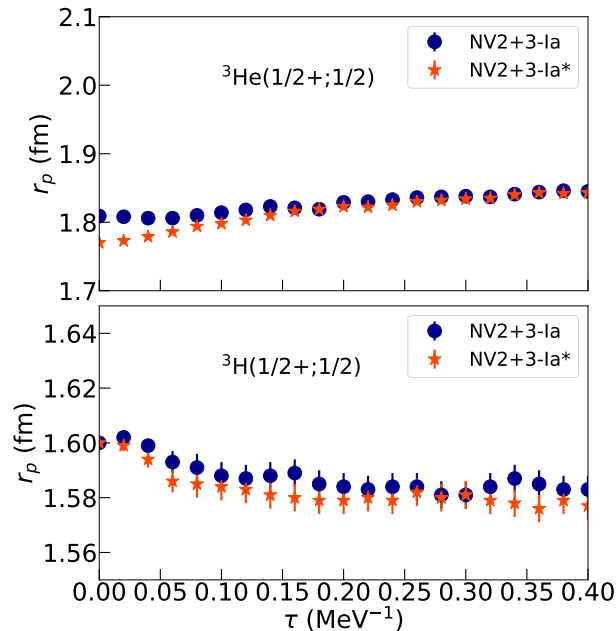

FIG. 2. The point proton rms radii for the ^{3}He and ^{3}H ground states as a function of imaginary time τ during GFMC propagation. Model Ia (blue circles) and model Ia* (orange stars) display similar behaviors for both systems.

In addition to the point proton rms radii, we include the GFMC energy propagations for the $A=6$ systems in Fig. 4. Note that the energies for both ^{6}Li(1^+; 0) and ^{6}He(0^+; 1) plateau near $\tau \simeq 0.1$ MeV^{-1}. The difference between the two models is not in the convergence behavior of the energy, but rather in its extrapolated value. While the energy values are well converged, the radius of the system is sensitive to small changes in the energy. Model Ia* predicts energies that are ~1 MeV higher than experimental values (see Table IV of Ref. [51]). In the case of ^{6}He, due to its close proximity to the $\alpha + 2n$ breakup threshold, this leads to clustering and an increased system size.

We also include an example of an electroweak matrix element propagation in Figure 5. We averaged starting from $\tau = 0.18$ MeV^{-1}, after spurious contamination had been removed from the wave functions and the matrix element was sufficiently converged. While terms like $e^{i\mathbf{q}\cdot\mathbf{r}_i}$ impact the overall size of the matrix element, the convergence behavior exhibited by the electroweak matrix element is not the same as that of the radius. Thus, we can safely extract the matrix elements after sufficient propagation in imaginary time τ.
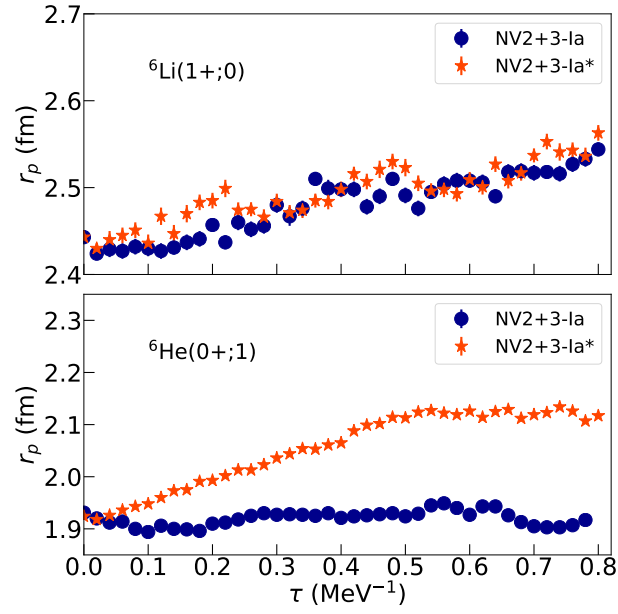
FIG. 3. The point proton rms radii for the ^{6}Li and ^{6}He ground states as a function of imaginary time τ during GFMC propagation. Model Ia (blue circles) and model Ia* (orange stars) display similar behaviors for ^{6}Li, but differ for ^{6}He. The model Ia* ground state of ^{6}He becomes much more diffuse than its counterpart.
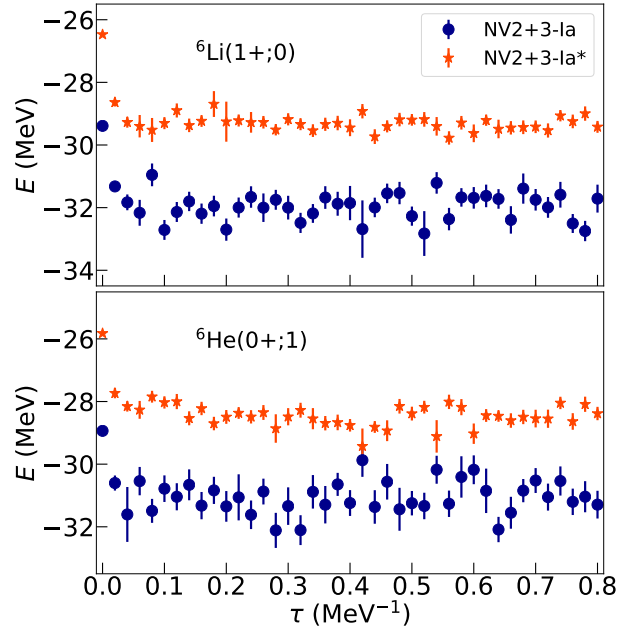

FIG. 4. The energy of the ^{6}Li and ^{6}He ground states as a function of imaginary time τ during GFMC propagation. The energies for both model Ia (blue ciricles) and model Ia* (orange stars) plateau near $\tau \simeq 0.1$ MeV^{-1}.

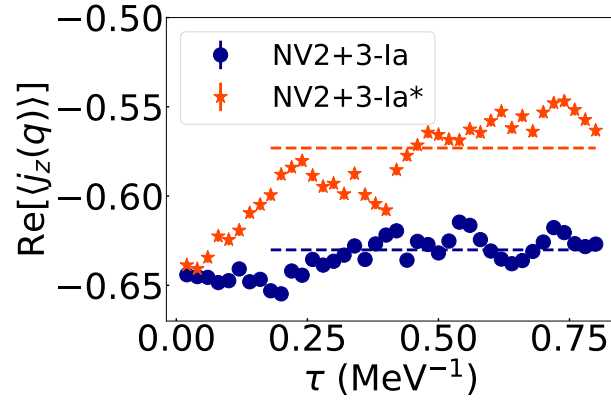FIG. 5. The GFMC propagation of the real component of the electroweak current operator j_z as a function of imaginary time τ using model Ia (blue circles) and model Ia* (orange stars). The dashed lines indicated the extrapolated value of the matrix element.